Journal of Alloys and Compounds 663 (2016) 885–898

Contents lists available at ScienceDirect

Journal of Alloys and Compounds

journal homepage: http://www.elsevier.com/locate/jalcom

Thermodynamic description of the AgCl–$CoCl_2$–$InCl_3$–NaCl system

Kun Wang [a, b, *], Christian Robelin [b], Zhu Wu [c], Chonghe Li [d], Leidong Xie [a], Patrice Chartrand [b]

[a] Shanghai Institute of Applied Physics, Chinese Academy of Sciences, Shanghai 201800, China
[b] Center for Research in Computational Thermochemistry (CRCT), Dept. of Chemical Engineering, Ecole Polytechnique, Montréal, Québec H3C 3A7, Canada
[c] Shanghai Institute of Microsystem and Information Technology, Chinese Academy of Sciences, Shanghai, 200050, China
[d] State Key Laboratory of Advanced Special Steel, Shanghai 200072, China

ARTICLE INFO

Article history:
Received 22 August 2015
Received in revised form
12 December 2015
Accepted 14 December 2015
Available online 17 December 2015

Keywords:
Chlorides
Phase equilibria
Thermodynamic properties
Phase transitions

ABSTRACT

Critical thermodynamic evaluations and optimizations of the AgCl–$CoCl_2$, AgCl–$InCl_3$, AgCl–NaCl, $InCl_3$–NaCl and $CoCl_2$–$InCl_3$ systems were carried out in the present work within the framework of the CALPHAD approach. The molten salt phase was described by the Modified Quasi-chemical Model, while the Compound Energy Formalism with various lattice ratios was used to treat the terminal solid solutions. The two binary double salts (Na_3InCl_6 and Ag_3InCl_6) were treated as the stoichiometric compounds of which Gibbs energies were modelled following the Neumann-Kopp rule. All the model parameters were optimized in terms of the required phase equilibria and thermochemical data arising from experimental measurements and theoretical predictions (First-principles method and empirical equation). A set of self-consistent thermodynamic database for the AgCl–$CoCl_2$–$InCl_3$–NaCl quaternary system was finally derived by merging the Gibbs energies for relevant phases in all binary systems (model parameters of $CoCl_2$–NaCl were adopted from the literature) based upon the Kohler–Toop interpolation technique in order to facilely calculate various phase equilibria and thermodynamic properties of the sub-ternary and quaternary systems. The calculated results involving multicomponent systems will support beneficial instructions in the related industrial processes.

1. Introduction

Molten salts are widely used in various industrial applications, especially where aqueous solutions have strong limitations. Such practical applications take advantage of the remarkable properties of fused salts like their thermal stability and generally low vapor pressure, being well adapted to nuclear applications and to the thermal energy storage and thermal medium in solar power systems [1,2]. Their wide potential window between decomposition limits allows the electro-winning of highly electropositive elements or the preparation of very electronegative elements [3,4]. Their ability to dissolve many inorganic compounds such as oxides, nitrides, carbides, and other salts makes them ideal solvents useful in electrometallurgy, metal coating, treatment of by-products, and energy conversion [5,6].

Research on phase equilibria and thermodynamic behavior is of primary importance in the search of the most suitable fused salts for specific applications. For instance, in development of molten salts based heat storage or transport media, the phase diagrams and thermodynamics will perform useful instructions in the screening of the system with higher fusion enthalpies and lower melting points [7]. For the preparation of cobalt dichloride graphite intercalation compounds from molten salts, a decisive role can be played by the phase diagrams in the choice between $CoCl_2$–NaCl and $CoCl_2$–KCl systems and imposing the melting compositions and temperatures of the intercalation process [8]. Therefore, it is preferable for the researchers to look over the related phase diagrams prior to their novel materials development.

Thermodynamic calculations through the CALPHAD approach are very effective in obtaining, with a limited amount of experimental data, the phase diagrams and related thermodynamic properties of multicomponent systems. To the best knowledge of the present authors, there has no such literature information for the AgCl–$CoCl_2$–$InCl_3$–NaCl quaternary system and its sub-ternary systems. The present work initially performed the thermodynamic assessments of the AgCl–$CoCl_2$, AgCl–$InCl_3$, AgCl–NaCl,

* Corresponding author. Shanghai Institute of Applied Physics, Chinese Academy of Sciences, Shanghai 201800, China.
E-mail address: wangkun@sinap.ac.cn (K. Wang).

http://dx.doi.org/10.1016/j.jallcom.2015.12.104
0925-8388/

$InCl_3$–NaCl and $CoCl_2$–$InCl_3$ systems on the basis of experimental data available in the literature and also theoretical data predicted from the first-principles method and empirical function. The entire binary model parameters assessed in the present work and literature [9] were then directly combined based upon the Kohler–Toop approach to derive a set of self-consistent thermodynamic functions for the AgCl–$CoCl_2$–$InCl_3$–NaCl quaternary system. Various phase equilibria and thermodynamic properties involving this system could thus be calculated by virtue of the presently derived thermodynamic database. Likewise, the interpolation technique and related binary parameters have also been adopted for successfully treating multi-phase equilibria in the AgCl–$CoCl_2$–$InCl_3$–KCl quaternary system in the accompanying article [10].

2. Data evaluation and prediction

Within the framework of the CALPHAD approach, the experimental phase equilibria and thermochemical data in literature should be evaluated and selected in detail, if lack of the relative information, theoretical predictions are sometimes performed, prior to the thermodynamic optimization, which will be introduced in the following section.

2.1. Review of literature data

2.1.1. Pure components

There are four terminal components but with five crystal modifications in the present system. The stable solid structures of pure AgCl and NaCl are halite, pure $InCl_3$ possesses $AlCl_3$ prototype, while $CoCl_2$ presents two different stable forms: $CdCl_2$-type modification at low temperature and an unknown structure at high temperature.

The melting point of AgCl ranges from 723 to 730 K in terms of binary AgCl-based phase diagrams. The fusion enthalpy of AgCl has been reported by Uvarov [11] to be 13.2 kJ/mol, while the fusion entropy proposed by Delaney [12] and Ushioda [13] to be $13 Jmol^{-1}K^{-1}$. The temperature-dependent thermodynamic functions for the solid and liquid AgCl were taken from the compilation of Barin [14] which shows the fusion enthalpy of 12.3 kJ/mol and fusion temperature of 730 K. It seems that there exhibits good agreement among reported fusion enthalpies, thus the fusion entropy proposed by Delaney [12] and Ushioda [13] may be inappropriate because it will result in the fusion temperature of AgCl as high as 1015 K.

According to Seifert [15] and Wojakowska [16], there are two different forms for solid $CoCl_2$. Seifert [15] has found a weak effect at 973 ± 5 K through differential thermal analysis indicating a second modification of $CoCl_2$. The melting point of $CoCl_2$ was detected to be 989 K. By means of DSC and conductometric measurements, Wojakowska [16] has confirmed the existence of the high-temperature allotropic phase of $CoCl_2$ ($CoCl_2$_S2). It was found that the melting process of $CoCl_2$ is preceded by a solid–state transition appearing about 20 K below the melting point of $CoCl_2$. Due to deconvolution of the thermograms, the enthalpy of fusion and that of solid–state transition were found to be 36.4 and 9.6 kJ mol^{-1}, respectively. Melting point of $CoCl_2$ was established to be 999.0 K. It is obvious that the polymorphic transition close to the melting temperature was hardly detected in most cases and the overall transition enthalpy of 46 kJ mol^{-1} between solid and liquid $CoCl_2$ (including solid transition and fusion) is more meaningful to be compared with other related experimental data. The previous work [9] has evaluated the Gibbs energy functions of $CoCl_2$ in solid and liquid phases but ignoring that of the high-temperature solid phase. The reported functions manifest that $CoCl_2$ is melted at 997 K with a fusion enthalpy of 43.9 kJ/mol, which agree well with the measured results by Wojakowska [16] in the case of an additive of enthalpies from the solid transition and fusion of $CoCl_2$. These functions were directly introduced in the present work to treat $CoCl_2$ss (low-temperature allotrope) and liquid phase. The $CoCl_2$_S2 phase was also considered in the present work whose Gibbs energy function was obtained by exerting a transition temperature of 977 K and transition enthalpy of 9.6 kJ/mol on the $CoCl_2$ss phase. This treatment inevitably raised the melting point of $CoCl_2$ up to 1002 K, but the temperature increment of 5 K still lies in a tolerance range for relevant measurements under the very high temperature.

The melting temperature of $InCl_3$ ranges from 849 to 875 K according to the $InCl_3$ based phase diagrams. The Gibbs energy function of solid $InCl_3$ was taken from the compilation of Glushko [17] while that of liquid $InCl_3$ is still lacking which will severely impede thermodynamic descriptions of the $InCl_3$ based molten salt system. However, the heat capacity of liquid $InCl_3$ has been reported by Glushko [17], and then the fusion enthalpy and temperature are just required to be integrated for the Gibbs energy function of liquid $InCl_3$. This requirement can be fulfilled by critically evaluating the slopes of $InCl_3$ liquidus in various $InCl_3$-based phase diagrams (see more details in the appendix).

NaCl is a very common salt used in various practical applications. Its melting point of 1073 K and fusion enthalpy of 28.16 kJ/mol are widely accepted in most thermochemical data compilations. Gibbs energy functions of this component in liquid and solid state were directly taken from the compilation of Barin [18].

2.1.2. The AgCl–$CoCl_2$ system

The complete phase diagram for the AgCl–$CoCl_2$ system has been solely determined by Krzyzak [19] through differential scanning calorimetry method. This system is simple and just of the eutectic type with the invariant point locating at 671 ± 2 K&19.5 mol% $CoCl_2$. The limited solid solubility of $CoCl_2$ in AgCl exists which does not exceed 2 mol%. Seifert [20] has measured various cobalt dihalide based phase diagrams, while just proposed a eutectic point of 673.15 K&20 mol%$CoCl_2$ for the AgCl–$CoCl_2$ system. It is clearly seen that the measured eutectic point from both of the investigators [19,20] are in satisfactory consistency. Also, excess enthalpies of binary liquid mixtures were just measured by Papatheodorou [21] at 1080 K through the single-unit high-temperature reaction calorimeter.

2.1.3. The NaCl–$InCl_3$ system

Phase diagrams for the NaCl–$InCl_3$ system have been experimentally determined by several research groups [22–26]. Vovkogon [23] has firstly established the whole phase diagram of this binary system through thermal analysis method. An intermediate compound $NaInCl_4$ was discovered and congruently melted at 1003.2 K. Two eutectic reactions were thus formed on both side of $NaInCl_4$ with the invariant points located at 20.97 mol%NaCl & 591.0 K and 61.03 mol% NaCl & 975.2 K, respectively. However, the existence of $NaInCl_4$ was not further confirmed and Na_3InCl_6 instead regarded as the only stable double salt in the later observations [22,24–26]. Fedorov [24] found that the double salt Na_3InCl_6 would be incongruently melted at 683.2 K in terms of the thermal analysis method. The peritectic composition corresponding to this temperature contains 54.64 mol% NaCl. This compound forms a eutectic reaction with $InCl_3$ that melts at 545.2 K and contains 51 mol% NaCl. Sryvtsev [25] has also observed Na_3InCl_6 incongruently melted but occurring at the temperature of 689.2 K with peritectic composition comprising 63.00 mol% of NaCl. The eutectic reaction is also formed from $InCl_3$ and Na_3InCl_6 but located at 51.00 mol%NaCl & 543.2 K. Chatova [22] has established the $InCl_3$–NaCl phase diagram in which Na_3InCl_6 was observed to be

congruently melted at 683.2 K. This melting point differs only by 2 K from the eutectic formed by the compound with NaCl. With $InCl_3$, it forms a eutectic point containing 49 mol% NaCl at 545.2 K. By virtue of DTA measurement, Afinogenov [26] has also constructed the NaCl–$InCl_3$ phase diagram for which the basic feature is similar to that proposed by Chatova [22] but with a lower NaCl liquidus. The crystal structure of Na_3InCl_6 at 200 K has been determined by Yamada [27] using the single-crystal X-ray analysis which belongs to the trigonal system with an isolated $InCl_6^{3-}$ anion and two crystallographically nonequivalent sodium ions Na(1) and Na (2). Currently, there still lack of the thermochemical data for the double salt and molten salt, and the existed phase equilibria data exhibit large discrepancies among various experimental measurements in the NaCl–$InCl_3$ system.

2.1.4. The AgCl–$InCl_3$ system

For AgCl–$InCl_3$ system, two groups of researchers [23,28] have conducted experimental investigations on the phase diagram by thermal analysis method. Both of the two groups have proved that this system includes an intermediate compound Ag_3InCl_6 and two eutectic reactions, but discrepancies still exist on the melting temperatures of the compound and eutectic points. Vovkogon [23] observed that Ag_3InCl_6 could be congruently melted at 646 K which is 15 K lower than the temperature reported by Fedorov [28]. A polymorphic transition of Ag_3InCl_6 at 608.2 K was firstly proposed by Fedorov [28] without any further confirmation. The larger controversial was indeed ascribed to the positions of the two eutectic points. The former reported that the two points were placed at 642 K & 77 mol% and 602 K & 32 mol% compared with 645 K & 61 mol% and 653 K & 79 mol% AgCl by the later, respectively. Up to now, there exist no experimental measurements on the crystal structure information and thermochemical data of the double salt (Ag_3InCl_6) and molten salt in the AgCl–$InCl_3$ system.

2.1.5. The AgCl–NaCl system

Equilibrium phase relations for the AgCl–NaCl system have been experimentally determined by three research groups [29–31]. All the investigations confirm that just two phases with liquid and solid solution are included in this binary system. By using the visual-polythermal method, Zhemchuzhnui [30] has firstly constructed the liquidus and solidus line under which there exhibits completely homogenous solid solution over the entire composition region. However, a miscibility gap (MG) was later detected by Stokes [31] for the solid phase with the upper critical point (UCP) near 448 K. The solid solubility boundary was determined by observing different optical morphologies for the samples, with completely transparent form above the boundary while milky-white opaque appearance below the boundary. This MG was later confirmed by Sinistri [29] through high temperature X-ray diffraction measurements with the sample preparation given particular care in order to describe as accurately as possible the limits of solid solubility boundary.

Large amounts of information are available in the literature on the thermochemical data of the solid and liquid phase in the binary AgCl–NaCl system. The enthalpies of mixing in the binary melts were measured at 933 K by Hersh [32] using high-temperature reaction calorimetry (both solid–liquid and direct liquid–liquid calorimetry) and at 1133 K by Murgulescu [33] employing the Pt calorimeter (direct liquid–liquid calorimetry). Activities of AgCl in the binary AgCl–NaCl melt were derived from electromotive force measurements (EMF) with galvanic cell (Ag|AgCl–NaCl melts|-graphite, Cl_2) by Guion [34] from 1073 to 1173 K at compositions of 0.05, 0.30.5 (mole fraction of AgCl, similarly hereinafter), by Stern [35] from 1014 to 1222 K at compositions of 0.0775, 0.0891, 0.1233, 0.2530, 0.3331, 0.5260, by Makarova [36] at temperatures of 723 K, 773 K, 823 K over a concentration range from 0.48 to 0.67, by Moser [37] from 950 to 1150 K at compositions of 0.2452, 0.3882, 0.5005, 0.5860, 0.6776, 0.7906, 0.9, by Panish [38] from 850 to 1200 K at compositions of 0.0313, 0.0978, 0.209, 0.351, 0.505, 0.550, 0.581, 0.615, 0.635, 0.646, 0.667, 0.755, 0.85, by Pelton [39] from 830 to 1200 K at compositions of 0.0515, 0.1032, 0.1043, 0.2058, 0.3580, 0.5080, 0.7073, 0.8548. By designing the cell type of Cu|Ag|CsCl–AgCl–NaCl melts|Cl_2(C)|Cu, Richter [40] initially intended to obtain activity coefficients of molten salts with three components while the activities of AgCl in the binary AgCl–NaCl melts at 1073 K was also measured when no amount of CsCl was left in the melts. The heats of formation of the solid solution in the AgCl–NaCl system were also determined at 623 K by Kleppa [41] using high-temperature solution calorimetry with pure liquid silver nitrate as the solvent and at temperatures of 648, 683, 723, 773, 823, 873 K by Nazarov [42] deriving from the experimental dependence of the activities of the components on the compositions. Activities of AgCl in the binary AgCl–NaCl solid solution, could also be achieved indirectly from EMF measurements with solid galvanic cell (C, Cl_2|AgCl–NaCl|AgCl|Cl_2, C) by Karpachev [43] at 713 K over wide concentration range, with solid cell (Pb, $PbCl_2$|AgCl–NaCl|Ag, AgCl) by Watcher [44] from 400 to 500 K at compositions of 0.160, 0.193, 0.296, 0.368, 0.440, 0.596, 0.601, 0.636, 0.719, 0.805, 0.870, with solid cell (Ag|AgCl|AgCl–NaCl|Ag) by Ptak [45] from 540 to 590 K at compositions of 0.1, 0.15, 0.2, 0.25, 0.5, 0.8, 0.85, 0.9, with solid cell (Ag|AgCl–NaCl|Cl_2,C) by Panish [38] from 495 to 1050 K at compositions of 0.0313, 0.0978, 0.209, 0.351, 0.505, 0.550, 0.581, 0.615, 0.635, 0.646, 0.667, 0.755, 0.850. It seems that the EMF values exhibit satisfactory convergence for the molten salt while great dispersion for the solid solution. The reason why the dichotomy happens will be discussed in detail in the following section of results and discussion.

2.1.6. The $CoCl_2$–$InCl_3$ system

Phase equilibria concerning the $CoCl_2$–$InCl_3$ system was only detected by Fedorov [46] through thermal analysis method. This system is also simple and just of the eutectic type but with a broad region of solid solutions appeared on both of the components. The two terminal solid solutions form eutectic with molten salts comprising 51 mol% of $CoCl_2$ at 798.2 K. As yet, there exist no measurements on the thermochemical information of the $CoCl_2$–$InCl_3$ system.

2.1.7. The $CoCl_2$–NaCl system

The phase diagram and thermodynamic properties for the $CoCl_2$–NaCl system have been solely calculated by Robelin [9] on the basis of the critical review and evaluation of the experimental data available in the literature. No solid solubility was reported on both of the end-member components. The double salt Na_2CoCl_4 was thermodynamically treated which shows a temperature range of stability from 622 to 638 K. The calculated eutectic point is located at 639 K and 62.6 mol% NaCl. The model parameters optimized by Robelin [9] for this binary system was adopted in the present work to derive a set of thermodynamic database for the $CoCl_2$–NaCl based multicomponent system.

2.2. First-principles methodologies

First-principles calculation can supplement thermodynamic modeling and parameter optimization by providing needed thermochemical data of individual phases when lacking of relative experiments. All first-principles calculations based upon density functional theory (DFT) in the present work were performed using the CASTEP module [47], as interfaced with Materials studio 6.0. Ultrasoft (USPP), norm-conserving (NCPP) and on the fly (OTFG)

potentials were adopted, along with the exchange-correlation functionals of the local density approximation (LDA) and the generalized gradient approximation (GGA) like PBE, RPBE, WC, PW91 and PBEsol, to examine the effect of different DFT methods on the predicted ground state of structures. Here, 9 electrons as valences for Na ($2s^2 2p^6 3s^1$), 13 for In ($4d^{10} 5s^2 5p^1$), 7 for Cl ($2s^2 2p^5$) were used within USPP potential, 9 for Na ($2s^2 2p^6 3s^1$), 3 for In ($5s^2 5p^1$), 7 for Cl ($2s^2 2p^5$) within NCPP potential, 9 for Na ($2s^2 2p^6 3s^1$), 13 for In ($4d^{10} 5s^2 5p^1$), 7 for Cl ($2s^2 2p^5$) within OTFG potential. During the CASTEP calculations, the structure relaxations and final static calculations were conducted by employing the plane wave energy cutoff of 1000 eV for NCPP, 450 eV for USPP, 650 eV for OTFG, the Monkhorst-Pack k-point meshes of 0.03 $Å^{-1}$, energy conversion threshold of 0.005 meV/atom, maximum displacement of 0.0005 Å and maximum force of 0.01 eV/Å, in order to yield a high accuracy for the energy and atomic displacements. Due to the lack of relative crystal structure information, the first-principles calculation failed to be performed on Ag_3InCl_6. Finally, the formation enthalpy of Na_3InCl_6 with reference to NaCl and $InCl_3$ can be obtained in an equation of the following form,

$$\Delta H = E_{tot}(Na_3InCl_6) - 3E_{tot}(NaCl) - E_{tot}(InCl_3) \quad (2)$$

where $E_{tot}(Na_3InCl_6)$, $E_{tot}(NaCl)$ and $E_{tot}(InCl_3)$ are the electronic total energy of the Na_3InCl_6, NaCl and $InCl_3$ compound in their ground state structure at T = 0 K, respectively. More details are displayed in the appendix for the predicted values of the electronic total energies and equilibrium volumes, and also the resulting formation enthalpies of Na_3InCl_6 based upon various DFT methods. Detailed discussions on the dependence of relative values on various DFT methods will also proceed in the appendix.

2.3. Empirical prediction for the mixing enthalpy in melts

There are no reported measurements for the mixing enthalpy of the $InCl_3$–NaCl melt, but it is possible to estimate it by an empirical method. This method is simple and just to find a relationship between the mixing enthalpy of binary melts and the ionic parameters (usually the function of the ionic parameters). As proposed by Robelin [48], the function of the ionic parameters is defined as the following equation,

$$\begin{aligned}\delta_{12} &= \left[\left(r_{Na}^{+} + r_{Cl}^{-}\right) - \left(r_{M}^{3+} + r_{Cl}^{-}\right)\right] \Big/ \left[\left(r_{Na}^{+} + r_{Cl}^{-}\right)\left(r_{M}^{3+} + r_{Cl}^{-}\right)\right] \\ &= \left(r_{Na}^{+} - r_{M}^{3+}\right) \Big/ \left[\left(r_{Na}^{+} + r_{Cl}^{-}\right)\left(r_{M}^{3+} + r_{Cl}^{-}\right)\right]\end{aligned} \quad (3)$$

where r_i is the ionic radius of i, whose values are taken for an octahedral geometry from the compilation of Shannon [49]. The available cations M^{3+} in the present case rely on whether or not there exist sufficient measurements for the mixing enthalpy of the NaCl-MCl_3 melts. After carefully searching the literature information, the experimental mixing enthalpy reported for the NaCl–$LaCl_3$ [50], NaCl–$CeCl_3$ [50], NaCl-$PrCl_3$ [51], NaCl-$NdCl_3$ [52], NaCl-$SmCl_3$ [53], NaCl-$GdCl_3$ [53], NaCl-$DyCl_3$ [54], NaCl–$TbCl_3$ [55], NaCl–$ErCl_3$ [53], NaCl-$YbCl_3$ [53], NaCl–$FeCl_3$ [56], NaCl–$AlCl_3$ [57] binary melts at 50 mol% MCl_3 are ultimately selected to evaluate their intrinsic correlation with the function of the ionic parameters δ_{12}. The dependence of the mixing enthalpies of various melts on their parameter δ_{12} clearly takes on a linear relationship in the present case. Thus, the mixing enthalpy of a 50 mol%NaCl-50 mol% $InCl_3$ melt at 1100 K was estimated with a value of −15.5 kJ/mol. It should be noted that the composition of 50 mol% MCl_3 was chosen since it corresponds to the approximate composition where the mixing enthalpy of the liquid is most negative in (MCl_3–NaCl) mixtures. More details can be found in the appendix for the used ionic radiuses of all the cations and anions and the correlations between δ_{12} and mixing enthalpies in respective melts.

3. Thermodynamic modelling

In the quaternary AgCl–$CoCl_2$–$InCl_3$–NaCl system, there are three types of phases like solid salt solution, double salt and molten salt. The phases considered are listed in table A3 in the appendix, along with the model used to describe their thermodynamic properties. All the unknown model parameters were optimized based upon the assessed data from experimental measurements and theoretical predictions through the FactSage thermodynamic software [58].

3.1. Lattice stabilities

In Section 2.1.1, the phase stabilities and thermodynamic properties of the pure components were reviewed and evaluated, and a set of reliable Gibbs energy functions were recommended to use in the present work. These functions can be expressed in an equation of the following form,

$$\begin{aligned}{}^{0}G_i^{\varphi} &= G_i^{\varphi} - H^{SER} \\ &= a + bT + cTln(T) + dT^2 + eT^3 + fT^{-1} + \sum_n g_n T^n\end{aligned} \quad (4)$$

where H^{SER} is the molar enthalpy of the stable element reference (SER) of the pure element in its stable state at 298.15 K, T is the absolute temperature, and a to f and g_n are coefficients, n stand for a set of integers. The appendix displays all the coefficients appeared in Eq. (4) for the corresponding compounds.

3.2. Thermodynamic modeling for the molten salt

The liquid solution was thermodynamically described by the Modified Quasi-chemical Model [59] which takes into account short-range ordering between nearest-neighbors on a lattice or sublattice. This model has been successfully applied to a variety of molten salt systems [9,48,56,57]. In the present work, owing to the sole anion of Cl^-, short-range ordering was treated by considering the relative numbers of second-nearest-neighbor cation–cation pairs. The model parameters are the Gibbs free energy of formation of the following pair,

$$(A - Cl - A)_{pair} + (B - Cl - B)_{pair} = (A - Cl - B)_{pair} \quad \Delta g_{A-Cl-B} \quad (5)$$

where A and B are two different cations. The model was initially developed in terms of nearest-neighbor pairs (A-B) for species mixing on one lattice. In the present work, since the anionic sublattice is occupied only by Cl^-, the model can be used directly to treat cation–cation pairs on the cationic sublattice. The pair A-Cl-B can thus be notated as A-B here, whose formation energy can be expanded as a polynomial,

$$\Delta g_{AB} = \Delta g_{AB}^{0} + \sum_{(m+n\geq 1)} X_{AA}^{m} X_{BB}^{n} g_{AB}^{mn} \quad (6)$$

where X_{AA} and X_{BB} are the mole fraction of A–A and B–B pairs, respectively. Δg_{AB}^{0} and g_{AB}^{mn} are usually expressed as a + bT with a and b optimized by the experimental data. The pair fraction is usually claimed as the internal variable which will make the Gibbs

energy function reach the minimum at the specific composition, temperature and pressure. The model requires a definition of the cation–cation coordination numbers Z^{A}_{AA}, Z^{B}_{BB}, Z^{A}_{AB}, Z^{B}_{AB} for a given binary system A, B/Cl. The composition of maximum short-range ordering in the A, B/Cl binary system is determined by the ratio of Z^{A}_{AB}/Z^{B}_{AB}. For example, the choice of $2Z^{Ag}_{AgCo} = Z^{Co}_{AgCo}$ (M : Ag, Na) assumes that there exist maximum short-range ordering (MSRO) near the M_2CoCl_4 composition, while $Z^{In}_{M:In} = Z^{M}_{M:In}$(M : Ag, Na, Co) indicates MSRO appeared close to the compositions of $MInCl_4$ for M = Ag, Na and of M_2InCl_5 for M = Co. For the AgCl–NaCl melt, it possesses no MSRO and can be approximately equal to the regular solution, the choice of $Z^{Na}_{NaAg} = Z^{Ag}_{NaAg}$ will make a flexible shift between the regular solution model and the modified quasi-chemical model. The values for the cation–cation coordination numbers defined in the present system can be found in the appendix.

Once all the binary model parameters Δg^{0}_{AB} and g^{mn}_{AB} have been determined, the Gibbs energy of ternary or higher order solution can be predicted from the binary model parameters using a proper interpolation technique, and small ternary model parameters are sometimes needed to accurately treat the solution. In this work, the liquid solutions contain the cations Ag^{+}, Na^{+}, Co^{2+}, In^{3+} which are divided into three groups, with Ag^{+} and Na^{+} entering the first group while Co^{2+} and In^{3+} second and third group, respectively, according to the same or different charge valences. In each ternary subsystem, when all three components belong to the same group or the three different groups, "Kohler-like" symmetric extrapolation is used, when the first two of them belong to the same group and the third is in the other group, "Toop-like" asymmetric extrapolation is applied, where the third component is considered as an asymmetric one. According to this symmetric/asymmetric dichotomy, the pair fraction X_{AA} and X_{BB} in Eq. (6) for multicomponent systems should be replaced by pair fractions ratios χ_{AB} and χ_{BA} which can be expressed in the form of the following equation [59],

$$\chi_{AB} = \sum_{i=A,P}\sum_{j=B,P} X_{ij} \Big/ \sum_{i=A,B,P,Q}\sum_{j=A,B,P,Q} X_{ij} \tag{7}$$

where P represents all values of P in A-B-P asymmetric ternary subsystems in which B is the asymmetric component, and Q represents all values of Q in asymmetric A-B-Q subsystems in which A is the asymmetric component. Followed by equation (7), the detailed expressions for various χ_{AB} and χ_{BA} are listed as Eq. 8–13 for the present system.

$$\chi_{AgCo} = \frac{X_{AgAg} + X_{NaNa} + X_{AgNa}}{X_{AgAg} + X_{NaNa} + X_{CoCo} + X_{AgNa} + X_{AgCo} + X_{NaCo}} \quad \chi_{CoAg} = \frac{X_{CoCo}}{X_{AgAg} + X_{NaNa} + X_{CoCo} + X_{AgNa} + X_{AgCo} + X_{NaCo}} \tag{8}$$

$$\chi_{AgIn} = \frac{X_{AgAg} + X_{NaNa} + X_{AgNa}}{X_{AgAg} + X_{NaNa} + X_{InIn} + X_{AgNa} + X_{AgIn} + X_{NaIn}} \quad \chi_{InAg} = \frac{X_{InIn}}{X_{AgAg} + X_{NaNa} + X_{InIn} + X_{AgNa} + X_{AgIn} + X_{NaIn}} \tag{9}$$

$$\chi_{AgNa} = \frac{X_{AgAg}}{X_{AgAg} + X_{NaNa} + X_{AgNa}} \quad \chi_{NaAg} = \frac{X_{NaNa}}{X_{NaNa} + X_{AgAg} + X_{AgNa}} \tag{10}$$

$$\chi_{CoIn} = \frac{X_{CoCo}}{X_{CoCo} + X_{InIn} + X_{CoIn}} \quad \chi_{InCo} = \frac{X_{InIn}}{X_{CoCo} + X_{InIn} + X_{CoIn}} \tag{11}$$

$$\chi_{CoNa} = \frac{X_{CoCo}}{X_{CoCo} + X_{NaNa} + X_{AgAg} + X_{CoAg} + X_{CoNa} + X_{AgNa}} \quad \chi_{NaCo} = \frac{X_{NaNa} + X_{AgAg} + X_{AgNa}}{X_{CoCo} + X_{NaNa} + X_{AgAg} + X_{CoAg} + X_{CoNa} + X_{AgNa}} \tag{12}$$

$$\chi_{NaIn} = \frac{X_{NaNa} + X_{AgAg} + X_{AgNa}}{X_{NaNa} + X_{InIn} + X_{AgAg} + X_{AgNa} + X_{AgIn} + X_{InNa}} \quad \chi_{InNa} = \frac{X_{InIn}}{X_{NaNa} + X_{InIn} + X_{AgAg} + X_{AgNa} + X_{AgIn} + X_{InNa}} \tag{13}$$

Due to the dearth of ternary phase equilibria and thermochemical information, any ternary interaction terms are thus not included in the present work.

3.3. Thermodynamic modeling for the solid solution

Three binary solid solution phases, notated by (AgNa)Cl, $CoCl_2$ss, $InCl_3$ss, are included in the present case which can be modeled as the Compounds Energy Formalism [60,61]. For the (AgNa)Cl phase, the components AgCl and NaCl can form a solid solution with continuously homogeneity range while little amount of $CoCl_2$(<2%) can be mixed in AgCl. There also exhibit broad homogeneity ranges of $CoCl_2$ in $InCl_3$ss and $InCl_3$ in $CoCl_2$ss phase. Herein, the model $(Ag^{+}, Na^{+}, Co^{2+}, Va)_1(Cl^{-})_1$ was adopted to thermodynamically describe the (AgNa)Cl phase while $(Co^{2+}, In^{3+})_1(Va, Cl^{-})_3$, $(Co^{2+}, In^{3+}, Va)_1(Cl^{-})_2$ selected to treat the $InCl_3$ss and $CoCl_2$ss phase, respectively. All the model expressions and their parameters deduction are discussed in detail in the appendix.

3.4. Thermodynamic modeling for the double salt

In the present work, only two double salts (Ag_3InCl_6 and Na_3InCl_6) are taken into account in the thermodynamic calculations of the AgCl–$InCl_3$ and $InCl_3$–NaCl systems. Both of them are stoichiometric whose Gibbs energies per mole are currently described in a form of the following equation,

$$G_{M_3InCl_6} = 3G^{0}_{MCl} + G^{0}_{InCl_3} + \Delta H_{M_3InCl_6} - T\Delta S_{M_3InCl_6} \tag{14}$$

where G^{0}_{MCl} and $G^{0}_{InCl_3}$ are Gibbs free energies of singles salts MCl (M: Ag, Na) and $InCl_3$, $\Delta H_{M_3InCl_6}$ and $\Delta S_{M_3InCl_6}$ represent the formation enthalpy and entropy of the double salt with reference to the constituent single salts, respectively. $\Delta H_{M_3InCl_6}$ and $\Delta S_{M_3InCl_6}$ are assumed to be independent of temperature in the present modeling indicating heat capacities of the double salts comply with the Neumann-Kopp rule. The formation enthalpies and entropies are model parameters which were optimized in the present work based upon phase equilibria information as well as thermochemical data from the first-principles prediction. The appendix will give quite a few discussions on the Neumann-Koop rule and its application to obtaining heat capacities of Ag_3InCl_6 and Na_3InCl_6.

4. Results and discussion

All the experimental data available in literature are critically evaluated based upon the experimental techniques and consistency

among the resultant experimental datum. The model parameters are obtained by simultaneously reproducing all the reliable experimental data of all binary systems within their experimental error limits. All model parameters used in the present work for the phases of molten salt, solid salt solutions, and double salts can be found in the appendix. For the $CoCl_2$–NaCl system, the model parameters optimized by Robelin [9] are directly taken and the calculated phase diagram is placed in the appendix without further elaborations. The detailed discussions below have been conducted on the present calculated results for the phase diagrams and thermodynamic properties in the binary, ternary and quaternary systems.

4.1. The AgCl–$CoCl_2$ system

The calculated AgCl–$CoCl_2$ phase diagram is displayed in Fig. 1 along with the experimental phase equilibria data of Krzyzak [19] and Seifert [20]. There appears limited solid solubility of $CoCl_2$ in (AgNa)Cl phase which has been treated as the CEF model like $(Ag^+, Co^{2+}, Va)_1(Cl)_1$ in the present work. Table 1 shows the invariant reactions and the compositions of the respective phases from both the present calculation and previous experimental measurements [19,20]. The calculated mixing enthalpies for the AgCl–$CoCl_2$ melts at 1080 K are given in Fig. 2 in comparison with the calorimetric data from Papatheodorou [21]. It is clearly manifested from Figs. 1–2 and Table 1 that the present calculation can well and consistently reproduce all the reported experimental data concerning phase diagram and thermodynamic properties for the AgCl–$CoCl_2$ system.

4.2. The NaCl–$InCl_3$ system

Several sets of phase equilibria data [22–26] have been reported for the NaCl–$InCl_3$ system but great scatters are clearly exhibited among them from these different measurements. Moreover, it is still unavailable for relative thermochemical data involving the double salt (Na_3InCl_6) and molten salt. A dilemma is thus posed as no experimental data are reliable enough to optimize the model parameters. To this end, two kinds of theoretical methods have been employed to aid model parameters optimization in the present work. One is the first-principles study being used to predict the formation enthalpy of Na_3InCl_6; the other is the empirical equation to obtain the maximum enthalpy of mixing for the molten salt. For the first-principles calculation, the accuracy of the prediction is significantly influenced by the selected parameters and various DFT methods. The formation enthalpy predicted by OTFG-PBESOL method was finally adopted to determine the model parameter $\Delta H_{Na_3InCl_6}$ (see more discussions in the appendix), and the remaining unknown parameter $\Delta S_{Na_3InCl_6}$ can be facilely optimized by means of the decomposition temperature of Na_3InCl_6. As described in detail in Section 2.3, an empirical method has been established to obtain the maximum enthalpy of mixing in the binary NaCl–$InCl_3$ melt of which value was finally predicted to be −15.5 kJ per mole salt at 1100 K. This value was adopted in the present case to determine the model parameter Δg_{InNa}. Based upon the model parameters evaluated above, the whole NaCl–$InCl_3$ phase diagram was calculated, as shown in Fig. 3. The calculated invariant points are also given in Table 2 in comparison with various measured values. It is obvious from the figure and table that the present calculation can well reproduce the liquidus data and decomposition temperature of Na_3InCl_6 from Fedorov [24] and Sryvtsev [25] while somewhat deviations apparently exist in the treatment of their reported eutectic reaction (liquid ↔ $InCl_3$+Na_3InCl_6), in particular the reaction temperature. The calculated result seems to approach more closely the data reported by Vovkogon [23]. It should be noted here that just one model parameter for the melt was employed to achieve such a good simulation of the NaCl–$InCl_3$ system.

4.3. The AgCl–$InCl_3$ system

Limited experimental data available in literature [23,28] are

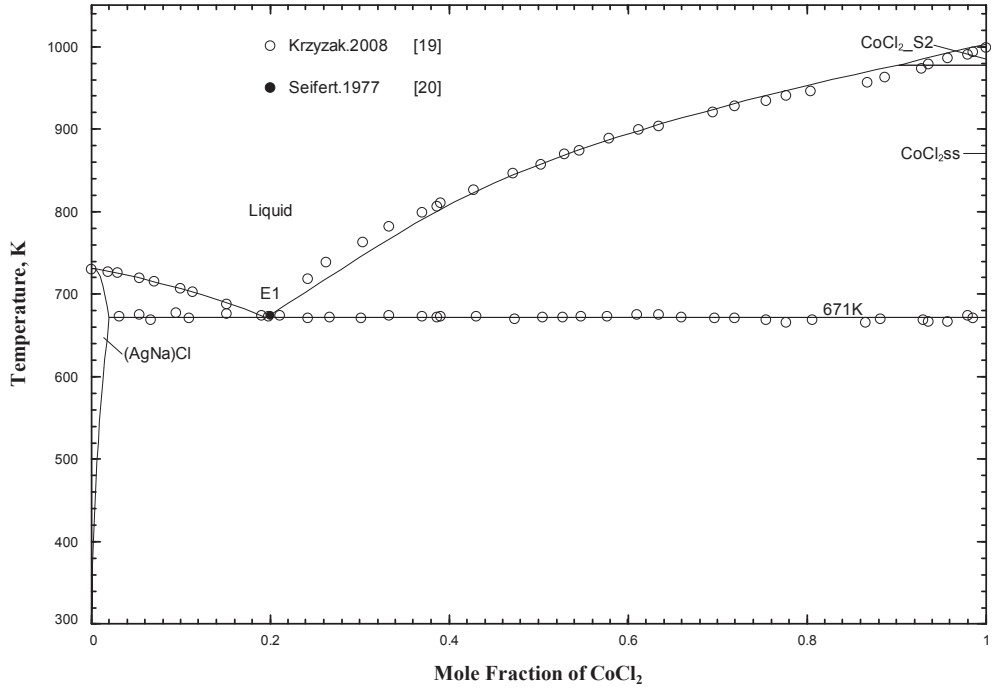

Fig. 1. The calculated AgCl–$CoCl_2$ phase diagram along with experimental data.

Table 1
Invariant point in the AgCl–$CoCl_2$ System (*: this work).

Reaction type	Temperature, K	Mole fraction of $CoCl_2$ (mol %)			Reference
		Phase#1	Phase#2	Phase#3	
$Liquid \overset{E1}{\leftrightarrow} AgCl + CoCl_2$	671.0	19.5	1.99%	100.00	[*]
	671.0	19.5	<2%	100.00	[19]
	673.2	20.0	–	–	[20]

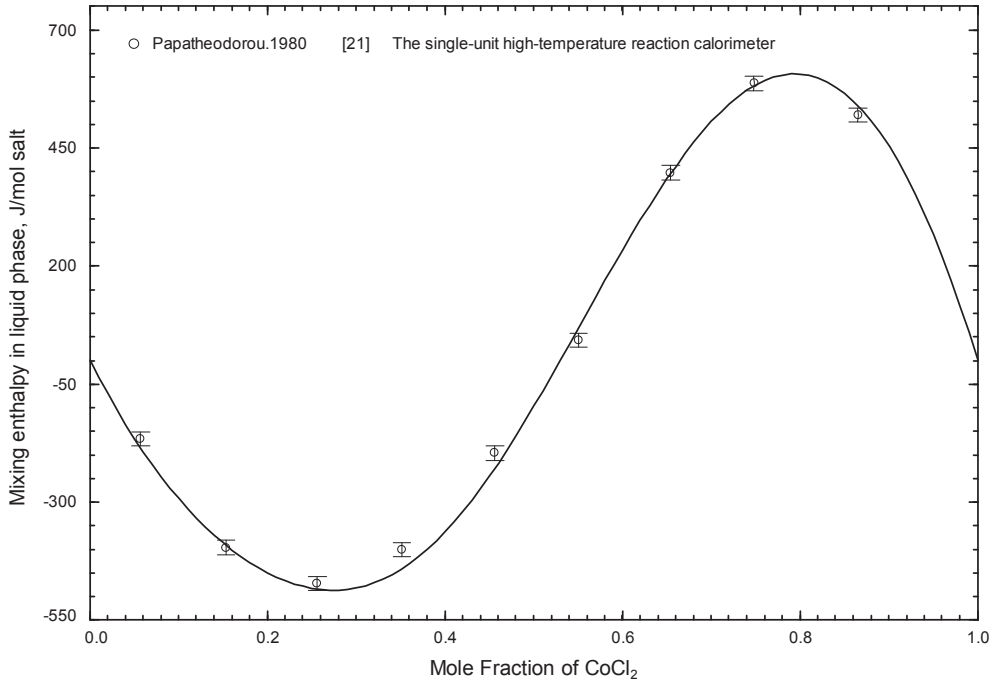

Fig. 2. The calculated mixing enthalpy in AgCl-$CoCl_2$ melts along with experimental data at 1080 K.

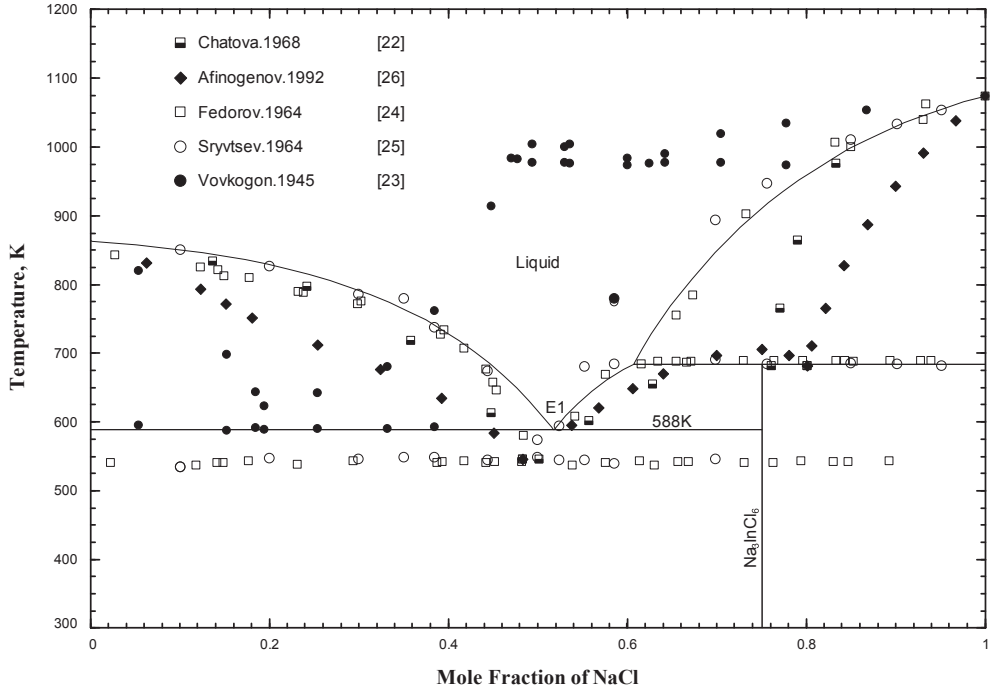

Fig. 3. The calculated NaCl–$InCl_3$ phase diagram along with experimental data.

Table 2
Invariant points in the NaCl–$InCl_3$ System (*: this work).

Reaction type	Temperature, K	Mole fraction of NaCl (mol %)			Reference
		Phase#1	Phase#2	Phase#3	
$Liquid \overset{E1}{\leftrightarrow} Na_3InCl_6 + InCl_3$	587.7	51.73	75.00	0.00	[*]
	545.2	49.00	75.00	0.00	[22]
	545.2	48.31	75.00	0.00	[26]
	545.2	51.00	75.00	0.00	[24]
	543.2	51.00	75.00	0.00	[25]
$Liquid \overset{E1}{\leftrightarrow} NaInCl_4 + InCl_3$	591.0	20.97	75.00	0.00	[23]
$Liquid + NaCl \overset{P1}{\leftrightarrow} Na_3InCl_6$	683.3	60.64	100.00	75.00	[*]
	683.2	54.64	100.00	75.00	[24]
	689.2	63.00	100.00	75.00	[25]
$Liquid \overset{E1}{\leftrightarrow} NaCl + Na_3InCl_6$	681.2	76.15	100.00	75.00	[22]
	681.3	80.09	100.00	75.00	[26]
$Liquid \overset{E1}{\leftrightarrow} NaCl + NaInCl_4$	975.2	61.03	100.00	50.00	[23]

solely related to the phase equilibria of the AgCl–$InCl_3$ system. As elaborated above, the theoretical methods can supplement key thermochemical data to aid in the model parameters optimization, but it is not the case for this system due to the lack of required crystal structure of Ag_3InCl_6 for the first-principles calculation and mixing enthalpies of AgCl-MCl_3 melts used in the empirical equation. Therefore, model parameters optimization was performed just according to the phase equilibria data of Vovkogon [23] and Fedorov [28] with more respect given to the eutectic temperatures determined by the latter. The whole phase diagram and invariant reactions for the AgCl–$InCl_3$ system with experimental data are shown in Fig. 4 and Table 3, respectively. The polymorphic transition of Ag_3InCl_6 failed to be treated in the present case due to lack of the transition enthalpy, while a prompt response could be made if measured the required data.

4.4. The $CoCl_2$–$InCl_3$ system

The calculated $CoCl_2$–$InCl_3$ phase diagram is presented in Fig. 5 in comparison with the only reported data from Fedorov [46]. This system is just of the eutectic type but with a broad region of solid solutions on both sides of the phase diagram. Two CEF models were constructed as $(Co^{2+}, In^{3+})_1(Cl^-, Va)_3$ and $(Co^{2+}, In^{3+}, Va)_1(Cl^-)_2$ with the former describing solid $InCl_3$ solution while the latter treating solid $CoCl_2$ solution. Table 4 shows the eutectic reaction and compositions of the respective phases from both the present calculation and experimental measurement [46]. It is evident from Fig. 5 and Table 4 that there exists fine consistency between the calculated results and experimental data in an aspect of phase equilibria. The empirical method mentioned in paragraph 2.3 also fails to predict the enthalpy of mixing in the $CoCl_2$–$InCl_3$ melts for there are no enough $CoCl_2$-MCl_3 systems providing the corresponding data. Herein, thermodynamic properties of the AgCl–$InCl_3$ and $CoCl_2$–$InCl_3$ melts from the present calculation are still under debate due to the dearth of thermochemical data used in the model parameters optimization. Nevertheless, massive thermodynamic calculations proved that the Modified Quasi-chemical Model can excellently simulate the configurational entropy of the

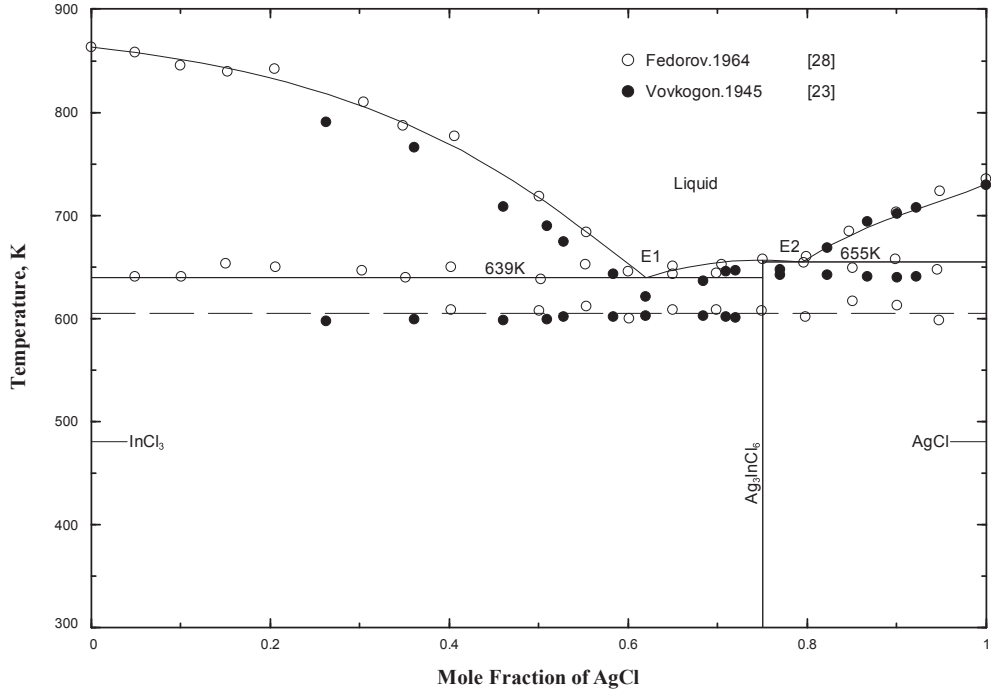

Fig. 4. The calculated AgCl–$InCl_3$ phase diagram along with experimental data.

Table 3
Invariant points in the AgCl–$InCl_3$ System (*: this work).

Reaction type	Temperature, K	Mole fraction of AgCl (mol%)			Reference
		Phase#1	Phase#2	Phase#3	
Liquid$\overset{E1}{\leftrightarrow}Ag_3InCl_6 + InCl_3$	639.3	61.93	75.00	0.00	[*]
	645.2	61.31	75.00	0.00	[28]
	602.0	64.34	75.00	0.00	[23]
Liquid$\overset{E2}{\leftrightarrow}Ag_3InCl_6 + AgCl$	654.7	79.50	75.00	100.00	[*]
	653.1	79.41	75.00	100.00	[28]
	641.7	80.83	75.00	100.00	[23]

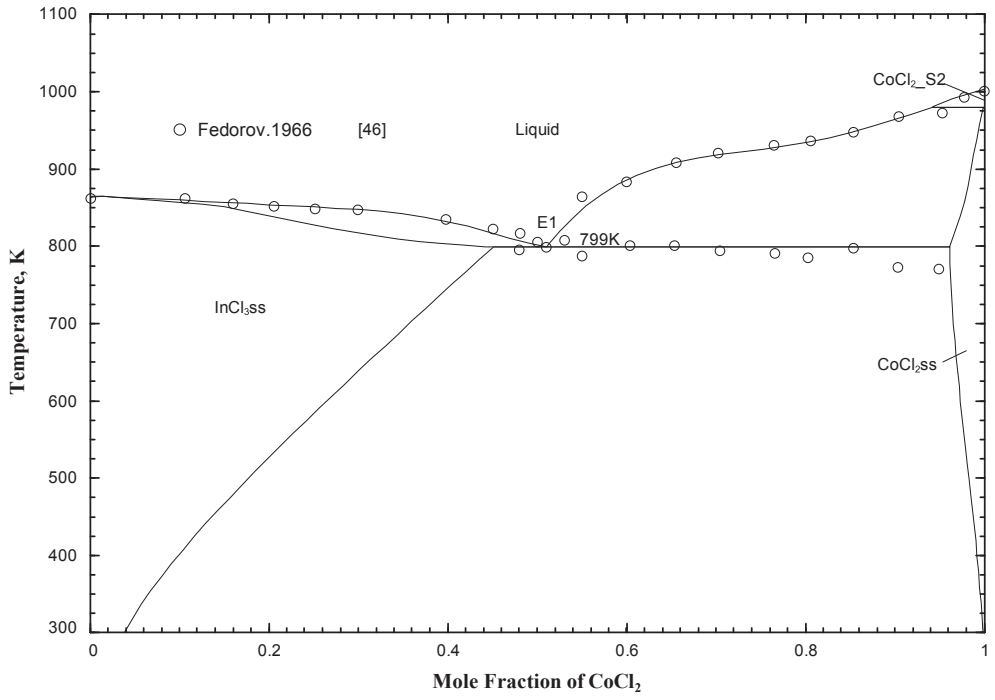

Fig. 5. The calculated $InCl_3$–$CoCl_2$ phase diagram along with experimental data.

Table 4
Invariant point in the $CoCl_2$–$InCl_3$ System (*: this work).

Reaction type	Temperature, K	Mole fraction of $CoCl_2$ (mol %)			Reference
		Phase#1	Phase#2	Phase#3	
Liquid$\overset{E1}{\leftrightarrow}CoCl_2 + InCl_3$	798.6	51.00	96.05	44.96	[*]
	798.2	51.00	96.00	45.00	[46]

solution phase. This leads to the possibility of accurately representing the mixing enthalpy and resultant thermodynamic properties just from phase diagram evaluations when these systems are as simple as possible like the present $InCl_3$ based phase diagrams.

4.5. The AgCl–NaCl system

There exists a wealth of experimental phase equilibria and thermochemical data [29–45] for the AgCl–NaCl system. After a critical evaluation on the experimental data, the phase diagram and thermodynamic properties of all phases are calculated in comparison with the relevant measured data. It can be seen from Fig. 6 that the calculated phase diagram well reproduces all the liquidus data while somewhat deviates from the solid solubility boundary of the miscibility gap. The boundary of miscibility gap could be satisfactorily described by endowing interaction parameters of the solid phase with a lower value, which, however, will be in a remarkable conflict with the mixing enthalpy of solid phase at 623 K reported by Kleppa [41]. It is well known that solid–solid phase equilibria are too hard to reach due to the sluggish diffusion kinetics of atoms or ions at low temperatures (UCP is 470 K for the present MG). High temperature data albeit of lesser precision are more likely to represent equilibrium than low temperature data even though of higher precision [62]. Therefore, major weight was allocated to the mixing enthalpy values of Kleppa [41] in the model parameters optimization for the solid phase. This treatment leads to the temperature of UCP rising to 580 K in the present calculation. Two sets of mixing enthalpy data [32,33] have been reported for the liquid phase while with great discrepancies. Major weight has also been assigned to the data from Hersh [32] for the tiny heat of mixing (lower than 150 J per mole salt) reported by Murgulescu [33] is

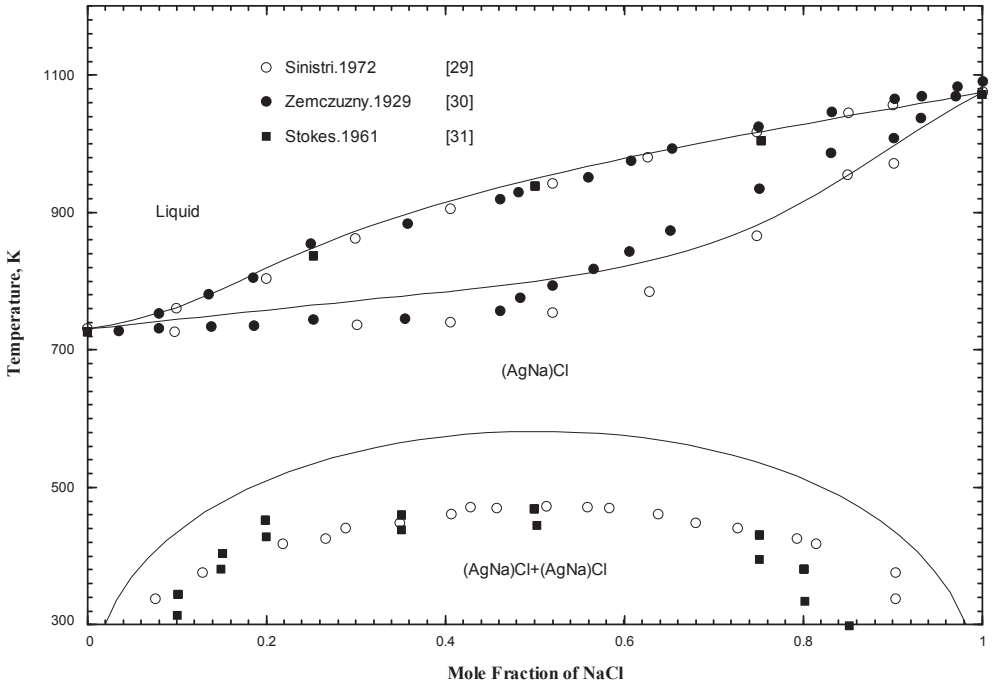

Fig. 6. The calculated AgCl–NaCl phase diagram along with experimental data.

too difficult to detect in normal techniques. Experimental data [34–40] concerning activities of AgCl in the melt were in good correspondence with each other and were all considered in the optimization. Unfortunately, experimental data [38,43–45] concerning activities of AgCl in the solid phase were in disagreement with each other and were even self-contradictory at low temperatures. This is mainly due to metastable equilibria in solid phases caused by the sluggish diffusion kinetics at low temperatures. Therefore, the present calculation can reasonably reproduce the activity data measured at higher temperatures due to relatively faster diffusion kinetics of atoms in solids. The appendix displays various types of property diagrams (activity vs temperature, activity vs composition, mixing enthalpy vs composition) calculated for the solid and liquid phase along with

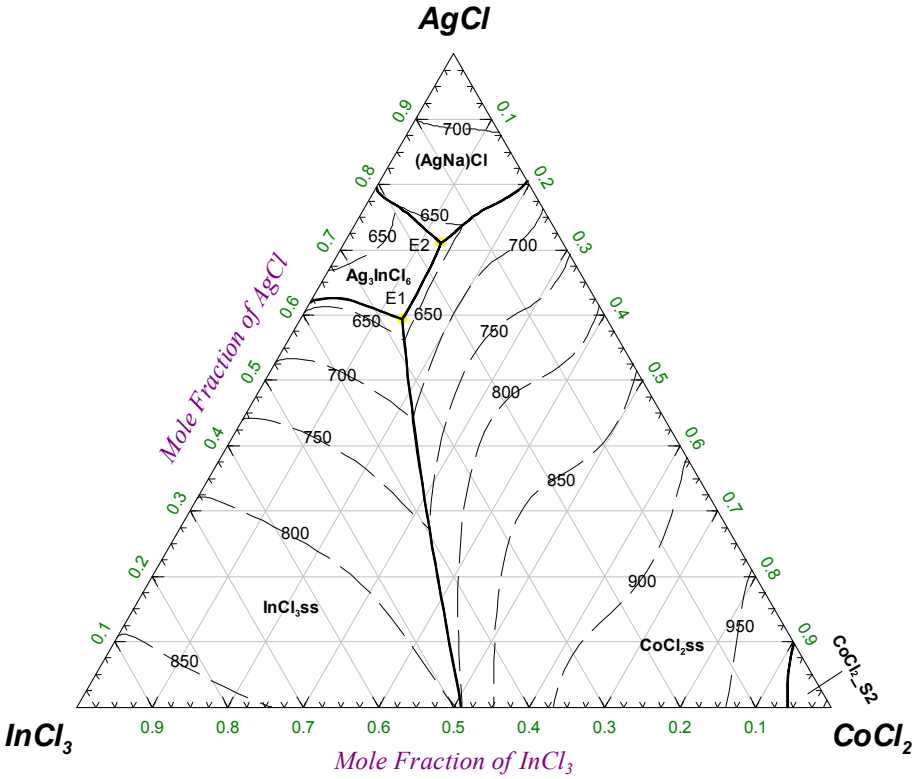

Fig. 7. The predicted liquidus projection of the AgCl–$CoCl_2$–$InCl_3$ system.

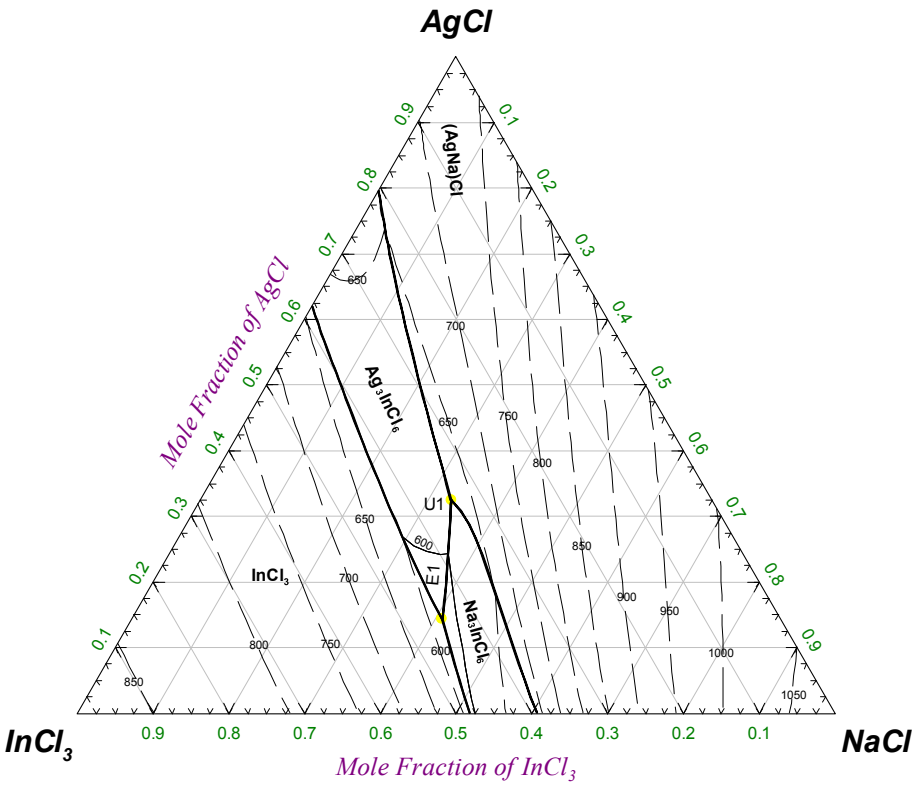

Fig. 8. The predicted liquidus projection of the AgCl–$InCl_3$–NaCl system.

large amounts of experimental data.

4.6. Ternary and quaternary systems

A set of self-consistent thermodynamic database was derived by directly merging all the binary model parameters for the relevant

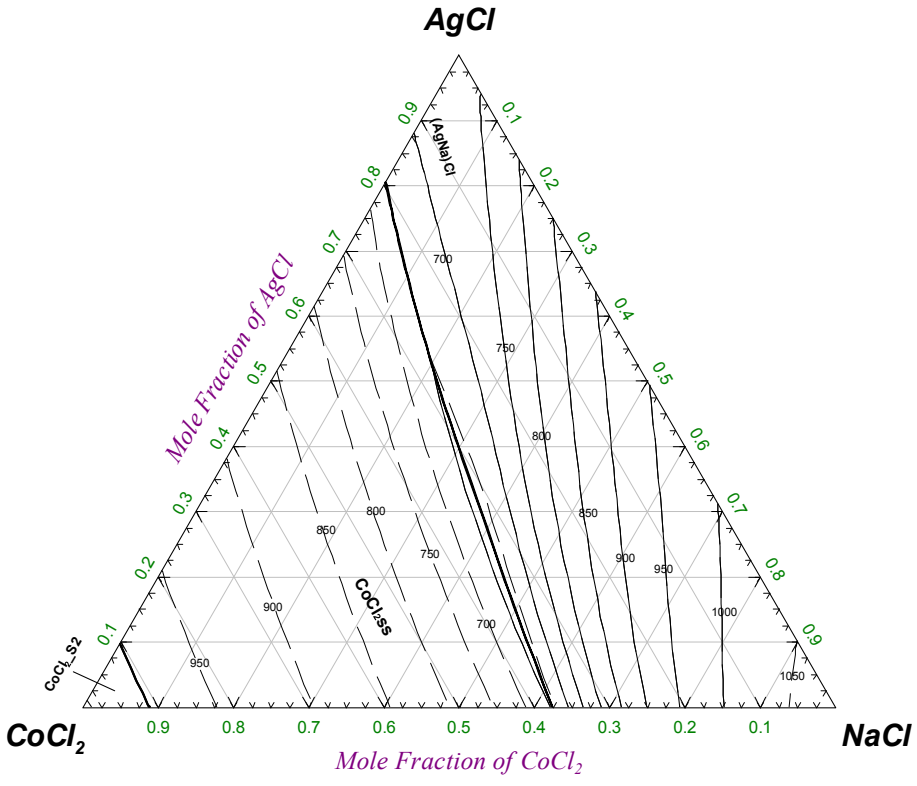

Fig. 9. The predicted liquidus projection of the AgCl–$CoCl_2$–NaCl system.

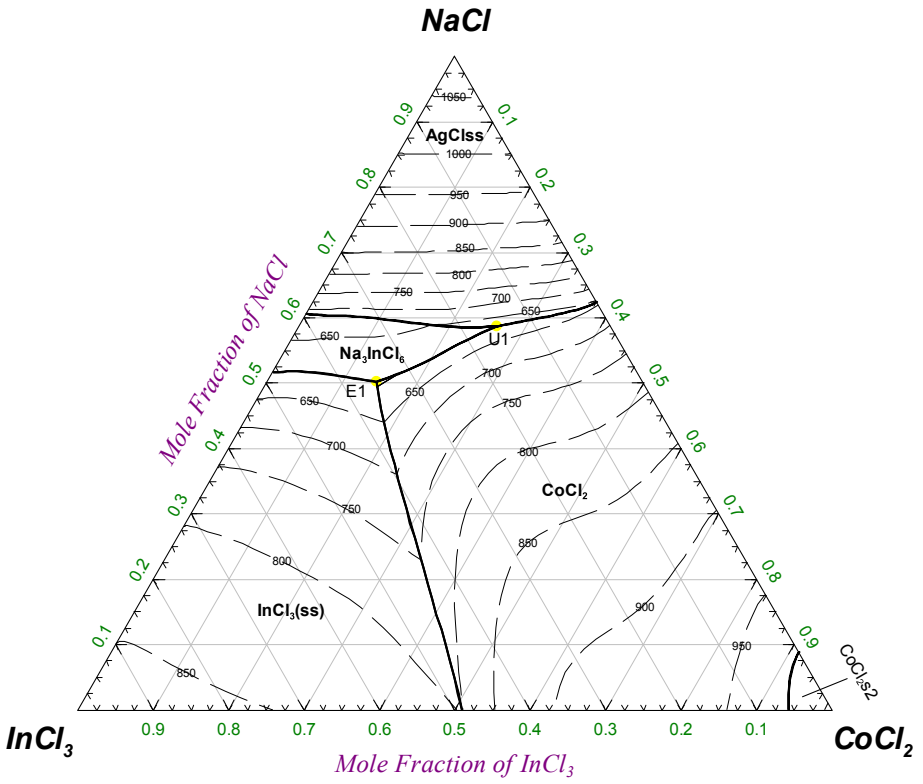

Fig. 10. The predicted liquidus projection of the $CoCl_2$–$InCl_3$–NaCl system.

Table 5
Invariant points in the AgCl–$CoCl_2$–$InCl_3$ System.

Reaction type	Temperature, K	Mole fraction of AgCl and $CoCl_2$ (mol%)							
		Phase#1		Phase#2		Phase#3		Phase#4	
Liquid$\overset{E1}{\leftrightarrow}Ag_3InCl_6+CoCl_2+InCl_3$	634.9	59.42	13.47	75.00	0.00	0.00	97.00	0.00	29.68
Liquid$\overset{E2}{\leftrightarrow}Ag_3InCl_6+CoCl_2+AgCl$	634.8	71.02	12.79	75.00	0.00	0.00	98.53	98.24	1.76

Table 6
Invariant points in the AgCl–$InCl_3$–NaCl System.

Reaction type	Temperature, K	Mole fraction of AgCl and NaCl (mol%)							
		Phase#1		Phase#2		Phase#3		Phase#4	
Liquid$\overset{E1}{\leftrightarrow}Ag_3InCl_6+Na_3InCl_6+InCl_3$	573.9	14.36	40.98	75.00	0.00	0.00	75.00	0.00	0.00
Liquid + AgCl$\overset{U1}{\leftrightarrow}Ag_3InCl_6+Na_3InCl_6$	611.2	34.62	32.08	82.85	17.15	75.00	0.00	0.00	75.00

Table 7
Invariant points in the $CoCl_2$–$InCl_3$–NaCl System.

Reaction type	Temperature, K	Mole fraction of NaCl and $CoCl_2$ (mol%)							
		Phase#1		Phase#2		Phase#3		Phase#4	
Liquid$\overset{E1}{\leftrightarrow}Na_3InCl_6+InCl_3+CoCl_2$	591.2	50.24	14.45	75.00	0.00	0.00	25.68	0.00	97.36
Liquid + NaCl$\overset{U1}{\leftrightarrow}Na_3InCl_6+CoCl_2$	614.8	58.73	26.27	98.28	1.72	75.00	0.00	0.00	99.06

phases in order to perform a serial of thermodynamic predictions on the phase equilibria and thermodynamic properties of the sub-ternary systems and the quaternary AgCl–$CoCl_2$–$InCl_3$–NaCl system. Figs. 7–10 show the calculated liquidus projections of the AgCl–$CoCl_2$–$InCl_3$, AgCl–$InCl_3$–NaCl, AgCl–$CoCl_2$–NaCl and $CoCl_2$–$InCl_3$–NaCl systems with the primary phases formed from the liquid phase in the process of solidification. The dotted lines in these figures are isotherms, with the numbers indicating the temperature in degree Kelvin. The predicted invariant points in these ternary systems are presented in Tables 5–7 (no ternary

Table 8
Predicted liquidus minima of the AgCl–$CoCl_2$–$InCl_3$–NaCl quaternary system.

Liquid composition, mol%			Fusion enthalpy, kJ/mol	Temperature, K
AgCl	NaCl	$CoCl_2$		
16.62	38.22	13.23	25.22	573.3
16.57	39.40	5.30	23.52	577.6
16.03	39.91	2.81	26.12	577.6
16.26	39.73	3.57	25.95	577.7

invariant point in AgCl–$CoCl_2$–NaCl system due to the crossing-type phase diagram). Table 8 shows liquidus minima in the AgCl–$CoCl_2$–$InCl_3$–NaCl system calculated by the Mesh Adaptive Direct Search algorithm integrated in FactSage software [63]. It is often of industrial interest, for the multicomponent system, to identify the low melting compositions at which local minima of the liquidus surface occur.

5. Conclusions

Critical thermodynamic evaluations and optimizations have been performed on the binary AgCl–$CoCl_2$, AgCl–$InCl_3$, $CoCl_2$–$InCl_3$, $InCl_3$–NaCl and AgCl–NaCl systems. The Modified Quasi-chemical Model was used to describe the molten salt phase, the CEF (Compound Energy Formalism) model with various lattice ratios applied to the solid salt solutions, while the double salts Ag_3InCl_6 and Na_3InCl_6 treated as stoichiometric compounds with Gibbs energies following the Neumann-Kopp rule, where the model parameters were optimized based on the experimental phase equilibria and thermochemical data available in the literature as well as the theoretical predictions (first-principles calculation and empirical atomic-parameter method). Comparisons of the calculated results with the experimental and predicted data show that the present work has reliably obtained the thermodynamic parameters of the five binary subsystems. With all these model parameters derived in this and previous work, the phase equilibria and thermodynamic properties in the quaternary AgCl–$CoCl_2$–$InCl_3$–NaCl system and its sub-ternary systems have been finally predicted according to the Kohler–Toop extrapolated model, which can be used to support theoretical guilds for the relative materials design.

Acknowledgments

Financial supports from the “Thorium Molten Salt Reactor” (TMSR), the “Strategic Priority Research Program” of the Chinese Academy of Sciences (XDA02002400), and the National Natural Science Foundation of China (Grant No. 21473234, 51374142) are gratefully acknowledged.

Appendix A. Supplementary data

Supplementary data related to this article can be found at http://dx.doi.org/10.1016/j.jallcom.2015.12.104.

References

[1] S.D. Stookev, J.S. Olcott, H.M. Garfinkel, Advances in class technology [M], Plenum Press, New York, N Y, 1962, pp. 397–411.
[2] C.O. Bolthrunis, Using molten salt to capture solar energy, Electron. Prog. 23 (1981) 25–28.
[3] S.Q. Jiao, D.J. Fray, Development of an inert anode for electrowinning in calcium chloride-calcium oxide melts, Metall. Mater. Trans. B 41B (2010) 74–79.
[4] O. Takeda, M. Li, M. Hoshi, Y. Sato, Electrowinning of lithium from molten salt containing LiOH for hydrogen storage and transportation, ECS Trans. 33 (2010) 455–462.
[5] T.R. Griffiths, V.A. Olkovich, S.M. akimov, I. May, C.A. Sharrad, J.M. Charnock, Reprocessing spent nuclear fuel using molten carbonates and subsequent precipitation of rare earth fission products using phosphate, J. Nucl. Mater. 418 (2006) 116–121.
[6] V.A. Volkovich, T.R. Griffiths, R.C. Thied, Treatment of molten salt wastes by phosphate precipitation: removal of fission product element after pyrochemical reprocessing of spent nuclear fuel in chloride melts, J. Nucl. Mater. 323 (2003) 49–56.
[7] D. Mantha, T. Wang, R.G. Reddy, Thermodynamic modeling of eutectic point in the $LiNO_3$-$NaNO_3$-KNO_3-$NaNO_2$ quaternary system, Sol. Energy Mater. Sol. Cells 118 (2013) 18–21.
[8] J.-Y. Tilquin, J. Fournier, D. Guay, J.P. Dodelet, G. Denes, Interaction of $CoCl_2$ into graphite: mixing method Vs molten salt method, Carbon 35 (1997) 299–306.
[9] Christian Robelin, Patrice Chartrand, Arthur D. Pelton, Thermodynamic evaluation and optimization of the (NaCl + KCl + $MgCl_2$ + $CaCl_2$ + $MnCl_2$ + $FeCl_2$ + $CoCl_2$ + $NiCl_2$) system, J. Chem. Thermodyn. 36 (2004) 809–828.
[10] K. Wang, Z. Fei, J. Wang, Z. Wu, C. Li, L. Xie, Thermodynamic description of the AgCl-$CoCl_2$-$InCl_3$-KCl system, Mater. Chem. Phys. 163 (2015) 73–87.
[11] N.F. Uvarov, E.F. Hairetdinov, V.V. Boldyrev, Correlations between parameters of melting and conductivity of solid ionic compounds, J. Solid State Chem. 51 (1984) 59–68.
[12] M.J. Delaney, S. Ushioda, Raman spectra of silver-halide melts and sublattice melting in the superionic conductor a-AgI, Phys. Rev. B Solid State 16 (1977) 1410–1415.
[13] S. Ushioda, M.J. Delaney, Liquid-like Raman scattering by superionic materials, Solid State Commun. 32 (1979) 67–70.
[14] I. Barin, Thermochemical data of pure substances, third ed., VCH Verlag GmbH, Weinheim, Germany, 1995, p. 6.
[15] H.J. Seifert, Alkali metal chloride-cobalt(II) chloride systems, Z. fuer Anorg. Allg. Chem. 307 (1960) 137–144.
[16] A. Wojakowska, E. Krzyak, S. Plinska, Melting and high-temperature solid state transactions in cobalt(II) halides, J. Therm. Anal. Calorim. 88 (2007) 525–530.
[17] Glushko Thermocenter of the Russian Academy of Sciences, IVTAN Association, Izhorskaya 13/19, 127412 Moscow, Russia, 1994.
[18] I. Barin, O. Knacke, O. Kubaschewski, Thermochemical Properties of Inorganic Substances, Springer-Verlag, Berlin, 1977, p. 519.
[19] E. Krzyzak, A. Wojakowska, Thermodynamics and phase equilibrium studies of silver halide-cobalt (II) halide systems, J. Therm. Anal. Calorim. 93 (2008) 721–726.
[20] H.J. Von, Seifert L. Staude, On the systems AJ/CoJ_2, and the kristallchemischen relations in the group of doppelhalogenide A_nCoX_{n+2} (X = Cl, Br, J), Z. Anorg. Allg. Chem. 429 (1977) 105–117.
[21] G.N. Papatheodorou, O.J. Kleppa, Excess enthalpies of binary liquid mixtures: silver chloride-cadmium, manganese, iron, and cobalt dichlorides, J. Chem. Thermodyn. 12 (1980) 807–809.
[22] V.L. Chatova, I.S. Morozov, Indium trichloride-iron(II)chloride-sodium chloride system, Zhurnal Neorg. Khimii 13 (6) (1968) 1645–1648.
[23] A.P. Vovkogon, Y.A. Fialkov, Physicochemical investigation of the systems indium chloride- chlorides of other metals. I. Thermal analysis, Zhurnal Obshchei Khimii 15 (1945) 903–910.
[24] P.I. Fedorov, Tsu-Liang Chang, Reaction of indium chloride with sodium chloride, Zhurnal Neorg. Khimii 9 (1) (1964) 231–232.
[25] V.A. Sryvtsev, E.S. Petrov, The composition diagram for the system $InCl_3$-NaCl, Izv. Sib. Otd. Akad. Nauk. SSSR Seriya Khimicheskikh Nauk. 1 (1964) 107–109.
[26] Y.P. Afinogenov, The ternary reciprocal displacement system $InCl_3$+3Na= 3NaCl+In, Russ. J. Inorg. Chem. 37 (1992) 1348–1349 translated from Zhurnal Neorganicheskoi Khimii.
[27] K. Yamada, K. Kumano, T. Okuda, Conduction path of the sodium ion in Na3InCl6 studied by X-ray diffraction and 23Na and 115In NMR, Solid State Ion. 176 (2005) 823–829.
[28] P.I. Fedorov, N.I. Il'ina, Interaction of the chlorides of indium, potassium, copper(I), silver, and thallium(I), Zhurnal Neorg. Khimii 9 (1964) 1207–1210.
[29] Cesare Sinistri, Riccardo Riccardi, Chiara Margheritis, Paolo Tittarelli, Thermodynamic properties of the solid systems silver chloride- sodium chloride and silver bromide- sodium bromide from miscibility gap measurements, Z. fuer Naturforsch. Teil Astrophys. Phys. Phys. Chem. 27 (1972) 149–154.
[30] S.F. Zhemchuzhnui, Melts of some silver halides with alkali halides, Zhurnal Rus. Fiziko Khimicheskago Obshchestva 153 (1916) 203–221.
[31] R.J. Stokes, C.H. Li, The Sodium Chloride-silver Chloride Alloy System, October, 1961. Office of Naval Research Project Nonr-2456(00) NR-032–451.
[32] L.S. Hersh, O.J. Kleppa, Enthalpies of Mixing in Some Binary Liquid Halide Mixtures, J. Chem. Phys. 42 (1965) 1309–1322.
[33] Ilie G. Murgulescu, Dumitru I. Marchidan, Cr Telea, Heat of mixing in binary systems of molten salts, Rev. Roum. Chim. 11 (9) (1966) 1031–1034.
[34] J. Guion, M. Blander, D. Hengstenberg, K. Hagemark, Thermodynamic treatment and electromotive force measurements of the ternary molten salt systems silver chloride-sodium chloride-potassium chloride and silver chloride-sodium chloride-cesium chloride, J. Phys. Chem. 72 (1968) 2086–2095.
[35] Kurt H. Stern, Electrode potentials in fused systems. IV. A thermodynamic and kinetic study of the AgC1-NaCl system, J. Phys. Chem. 62 (1958) 385–390.
[36] N.L. Makarova, A.A. Nazarov, Thermodynamic properties of molten ternary system silver chloride-sodium chloride-lead chloride, Zhurnal Fiz. Khimii 40 (1966) 2117–2124.

[37] Z. Moser, W. Gasior, K. Rzyman, Activities and surface tension of liquid AgCl-NaCl solutions, J. Electrochem. Soc. Electrochem. Sci. Technol. 126 (1979) 1467–1470.
[38] M.B. Panish, F.F. Blankenship, W.R. Grimes, R.F. Newton, Thermodynamic properties of molten and solid solutions of silver chloride and sodium chloride, J. Phys. Chem. 62 (1958) 1325–1331.
[39] A.D. Pelton, S.N. Flengas, Thermodynamics of molten silver chloride- alkali chloride solutions by electromotive force measurements, J. Electrochem. Soc. 117 (1970) 1130–1140.
[40] Joachim Richter, Activity coefficients of molten salts with three components, Z. fuer Naturforschung Teil Astrophys. Phys. Phys. Chem. 26 (1971) 1031–1035.
[41] O.J. Kleppa, S.V. Meschel, Heats of Formation of Solid Solutions in the Systems (Na-Ag)Cl and (Na-Ag)Br, J. Phys. Chem. 69 (1965) 3531–3537.
[42] A.A. Nazarov, Thermodynamic properties of AgCl-NaCl solid solutions, Zhurnal Fiz. Khimii 39 (1965) 1451–1457.
[43] S.V. Karpachev, V.P. Obrosov, Thermodynamic properties of solid solutions of silver chloride and sodium chloride, Elektrokhimiya 4 (1968) 1096–1099.
[44] A. Wachter, Thermodynamic properties of solid solutions of silver chloride and sodium chloride, J. Am. Chem. Soc. 54 (1932) 919–928.
[45] Wladyslaw Ptak, Jerzy Nowakowski, Thermodynamic investigations of a silver chloride and sodium chloride system by measurement of the emf. of concentration cells, Arch. Hut. 17 (1972) 125–142.
[46] P.I. Fedorov, N.I. Il'ina, Reaction of indium chloride with the chlorides of iron, cobalt, and bismuth, Zhurnal Neorg. Khimii 11 (1) (1966) 205–207.
[47] S.J. Clark, M.D. Segall, C.J. Pickard, P.J. Hasnip, M.J. Probert, K. Refson, et al., First principles methods using CASTEP, Z. fuer Kristallogr. 220 (2005) 567–570.
[48] C. Robelin, P. Chartrand, Thermodynamic evaluation and optimization of the (NaCl +KCl+$MgCl_2$+$CaCl_2$+$ZnCl_2$) system, J. Chem. Thermodyn. 43 (2011) 377–391.
[49] R.D. Shannon, Revised effective ionic radii and systematic studies of interatomic distances in halides and chalcogenides, Acta Crystallogr. A A32 (1976) 751–767.
[50] S. Yimin, PhD thesis, Beijing Univ. Science and Technology, (1999).
[51] M. Gaune-Escard, L. Rycerz, W. Szczepaniak, A. Bogacz, Calorimetric investigation of $PrCl_3$-NaCl and $PrCl_3$-KCl liquid mixtures, Thermochim. Acta 236 (1994) 59–66.
[52] M. Gaune-Escard, A. Bogacz, L. Rycerz, W. Szczepaniak, Calorimetric investigation of $NdCl_3$-MCl liquid mixtures (where M is Na, K, Rb, Cs), Thermochim. Acta 236 (1994) 67–80.
[53] F. Dienstbach, R. Blachnik, Enthalpies of mixing of fused alkali metal halide-lanthanide halide systems, Z. fuer Anorg. Allg. Chem. 412 (1975) 97–109.
[54] M. Gaune-Escard, Enthalpies of mixing in the $DyCl_3$-NaCl, $DyCl_3$-KCl and $DyCl_3$-$PrCl_3$ liquid systems, J. Alloys Compd. 204 (1994) 185–188.
[55] L. Rycerz, Mixing enthalpy of $TbCl_3$-MCl mixtures (M=Li, Na, K, Rb, Cs), High. Temp. Mater. Process. 2 (1998) 483–496.
[56] C. Robelin, Master's thesis, Ecole Polytechnique, Montreal, 1997.
[57] C. Robelin, P. Chartrand, A.D. Pelton, Thermodynamic evaluation and optimization of the NaCl-KCl-$AlCl_3$ system, J. Chem. Thermodyn. 36 (2004) 683–699.
[58] C.W. Bale, P. Chartrand, S.A. Degterov, G. Eriksson, K. Hack, R. Ben Mahfoud, J. Melancon, A.D. Pelton, S. Petersen, FactSage thermochemical software and databases, CALPHAD 26 (2002) 189–228.
[59] A.D. Pelton, P. Chartrand, The modified quasi-chemical model: part II. Multicomponent solutions, Metall. Mater. Trans. A 32 (2001) 1355–1360.
[60] M. Hillert, The compound energy formalism, J. Alloys Compd. 320 (2001) 161–176.
[61] M. Hillert, L. Kjellqvist, H. Mao, M. Selleby, B. Sundman, Parameters in the compound energy formalism for ionic systems, Calphad 33 (2009) 227–232.
[62] J.C. Zhao, Methods for Phase Diagram Determination (Edit), Elsevier Ltd, 2007, p. 19.
[63] Aimen E. Gheribi, Christian Robelin, Sébastien Le Digabel, Charles Audet, Arthur D. Pelton, Calculating all local minima on liquidus surfaces using the FactSage software and databases and the mesh adaptive direct search algorithm, J. Chem. Thermodyn. 43 (2011) 1323–1330.